First-principles investigation for $M(CO)_n/Ag(110)$ (M=Fe, Co, Ni, Cu, Zn, and Ag; n=1, 2) systems: Geometries, STM images, and vibrational frequencies

Lan-Feng Yuan, Jinlong Yang,* Qunxiang Li, Qing-Shi Zhu
Open Laboratory of Bond Selective Chemistry, University of Science and Technology of China, Hefei, Anhui 230026, P.R. China
(Received 20 June 2001; revised manuscript received 13 August 2001; published 28 December 2001)

Fe, Cu atoms and CO molecules were manipulated with a scanning tunneling microscope (STM) on a Ag(110) surface, and one or two CO can transfer from the surface and bond with a metal atom through the STM tip [H. J. Lee and W. Ho, Science **286**, 1719 (1999); Phys. Rev. B **61**, R16347 (2000)]. We perform a density-functional cluster model investigation for the systems. The experimental geometries are validated and understood using the frontier orbital theory. The STM topographic images are reproduced. The vibrational frequencies of the adsorbate systems are obtained by diagonalizing the second-derivative matrices and are in excellent agreement with the experimental measurements. The geometries and C-O stretch frequencies are predicted for systems with the adsorbate metal atom being Co, Ni, Zn, and Ag. These systems can be divided to two classes, and each class exhibits a different set of properties.

DOI: 10.1103/PhysRevB.65.035415 PACS number(s): 68.35.Ja, 68.37.Ef, 73.20.Hb, 82.65.+r

To freely manipulate individual molecules and atoms is a splendid goal for physicists and chemists. There are several possible roads which lead to this aim: for example, local mode vibrations,[1] laser optimal control of the molecular dynamics,[2] and scanning tunneling microscope (STM) technology.[3] Great progress had been made by STM due to its ability to observe and manipulate individual atoms and molecules.[4–7] Electronic tunneling between a STM tip and a molecule absorbed on a surface can induce intrinsic molecular motions, such as desorption[8–10] and rotation.[7,11,12] Dissociation of single molecules had been accomplished on both metal[13] and semiconductor[14] surfaces. Lately, even vibrational spectroscopy on single molecules became available using inelastic electron tunneling spectroscopy (IETS) with STM.[15,16] All these experiments improved the microscopic understanding of the mechanism and dynamics of surface chemistry, but no bond formation was involved.

Recently, Lee and Ho succeeded in controlled single-bond formation and characterization at the spatial limit with a STM.[17] In their experiment, individual iron atoms were evaporated and coadsorbed with CO molecules on a silver (110) surface at 13 K. A CO molecule was transferred from the surface to the STM tip and bonded with an Fe atom to form Fe(CO). A second CO molecule was similarly transferred and bonded with Fe(CO) to form $Fe(CO)_2$. The steps involved were visualized in a sequence of STM topographical images. Employing STM-IETS, they measured the C-O stretch vibrational frequencies of Fe(CO) and $Fe(CO)_2$ and the isotopic shifts of the frequencies owing to ^{13}C and ^{18}O. Most recently, Lee and Ho extended their experiment to the $Cu(CO)_n/Ag(110)$ (n=1,2) systems.[18] They found that the geometries of Cu(CO) and $Cu(CO)_2$ on Ag(110) are different from those of Fe(CO) and $Fe(CO)_2$.

In the interest of comprehending this important progress of single-molecule science, we perform first-principles calculations. The experimental geometries are validated and comprehended in terms of the frontier orbital theory (FOT). The STM topographical images are reproduced. A more exciting outcome is that the vibrational frequencies by IETS are obtained. Besides, the geometries and frequencies of the systems with other adsorbate metal atoms are predicted. The metal atoms can be divided into two classes, and each class exhibits a different set of properties.

The calculations are performed based on the linear combination of atomic orbital and molecular orbital (LCAO-MO) method. The atomic orbitals are represented by a double-numeric quality basis set with polarization functions (DNP), which are comparable to Gaussian 6-31G** sets. In this work, the local density approximation (LDA) to the density functional theory is employed, with the Vosko-Wilk-Nusair parametrization of the local exchange-correlation energy.[19] To improve the calculated binding energies, the generalized gradient approximation (GGA) is also used, with the Becke exchange gradient correction[20] and the Perdew-Wang correlation gradient correction.[21] Spin-unrestricted wave functions are employed. All calculations are carried out using the molecular simulation package DMOL.[22]

Cluster models had been successfully used to simulate adsorbate systems.[23,24] When a M (Fe or Cu) atom is adsorbed on Ag(110), it is located at a fourfold hollow site. Taking the nearest and next-nearest Ag neighbors of the M

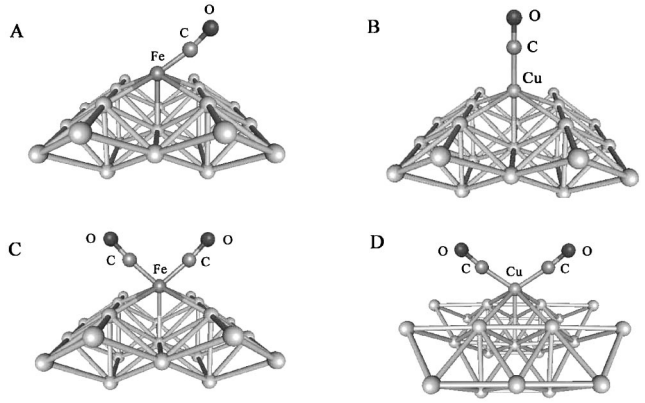

FIG. 1. Clusters simulating the systems on Ag(110). (A) $Fe(CO)Ag_{21}$ (TL geometry). (B) $Cu(CO)Ag_{21}$ (TS geometry) (C) $Fe(CO)_2Ag_{21}$ (SL geometry). (D) $Cu(CO)_2Ag_{21}$ (SS geometry).

TABLE I. Binding energies (eV) of the optimized systems relevant to $M(CO)$ and $M(CO)_2$ (M=Fe, Cu) on Ag(110).

Cluster	LDA E_b		GGA E_b	
CO	−12.62		−11.60	
Ag_{21}	−43.13		−26.79	
	Fe	Cu	Fe	Cu
MAg_{21}	−46.15	−46.95	−28.95	−29.84
$M(CO)Ag_{21}$ (TL)	−62.64	−61.22	−43.45	−42.46
$M(CO)Ag_{21}$ (TS)	−62.02	−61.16	−42.75	−42.46
$M(CO)Ag_{21}$ (Per)	−61.55	−61.23	−42.31	−42.49
$M(CO)_2Ag_{21}$ (SL)	−78.32	−74.80	−57.31	−53.92
$M(CO)_2Ag_{21}$ (SS)	−78.01	−75.36	−56.92	−54.73

TABLE II. Geometric parameters (bond lengths in Å and bond angles in degree) of the LDA optimized systems relevant to $M(CO)$ and $M(CO)_2$ (M=Fe, Cu) on Ag(110). β is the M-C-O bond angle, and τ is the angle between the [110] direction and the M-C bond. There are two points noteworthy. One is that the nearest Ag atom of the metal atom is on the second layer, not on the first layer. The other is that the direction of the M-C-O angle for Fe(CO), $Fe(CO)_2$, and $Cu(CO)_2$ is backed to the Ag(110) surface, contrary to the diagrams in Refs. 17 and 18.

Cluster	$r(M$-C)	r(C-O)	$r(M$-nearest Ag)	β	τ
$Fe(CO)Ag_{21}$	1.73	1.19	2.59	167.1	55.0
$Cu(CO)Ag_{21}$	1.80	1.16	2.57	180.0	0.0
$Fe(CO)_2Ag_{21}$	1.73	1.18	2.61	172.0	58.7
$Cu(CO)_2Ag_{21}$	1.81	1.16	2.72	173.1	56.2

atom, we obtain a cluster model with 21 Ag atoms. After a CO molecule is connected to the M atom, there are many conceivable orientations of CO. We consider three kinds. First, the CO is tilted and the M-C-O plane is parallel to the [001] direction, which is along the long margins of the rectangle consisting of the 4 Ag atoms in the first layer bonded with M directly. We denote this geometry as ''TL'' to emphasize ''tilted'' along the ''long margins,'' and its point group is C_s with the M-C-O plane as the only symmetry element. Second, the CO is tilted and the M-C-O plane is parallel to the $[1\bar{1}0]$ direction, which is along the short margins of the rectangle (denoted as ''TS'' in a like manner). Its point group is also C_s. Third, the M, C, and O atoms are in a straight line perpendicular to the surface (Per), and the point group is C_{2v} with the M-C-O line as the C_2 axis. The TL and Per geometries correspond to the experimental ones of the Fe(CO) and Cu(CO) systems, respectively,[17,18] and are shown in Figs. 1(a) and 1(b). After two CO molecules are bonded, Lee and Ho found that they are always symmetrically located,[18] but the M-C-O plane is parallel to the [001] direction for Fe [denoted as ''SL'' to emphasize ''symmetrically located'' and ''long margins,'' Fig. 1(C)] and the $[1\bar{1}0]$ direction for Cu [SS, Fig. 1(D)]. These two geometries are of the C_{2v} symmetry. We consider them for both Fe and Cu. In all optimization processes, the Ag atoms which do not connect directly with the adsorbate atom are fixed at their surface positions.[25]

The binding energies of the optimized systems are listed in Table I. Our computations successfully validate all the experimental geometries, which prove that the cluster sizes are enough. The geometric parameters of the four LDA-optimized clusters are given in Table II.

The observed different orientations of the adsorbate systems can be understood using the FOT.[26] We found that one or more metal atomic orbitals of each metal carbonyl contribute most to determining its orientation on Ag(110). The orbitals are $3d_{xz}$ for Fe(CO), $4s$ and $3d_{z^2}$ for Cu(CO), $3d_{xz}$ and $3d_{yz}$ for $Fe(CO)_2$, and $4p_x$ and $4p_y$ for $Cu(CO)_2$, where the z direction is the M-C axis. These orbitals are selected due to their relatively large weights in the frontier molecular orbitals and their ability to distinguish bondings with the Ag atoms at different orientations. The Cu $4s$ and $3d_{z^2}$ orbitals in Cu(CO) occupy 50% and 80% in the highest-occupied molecular orbit (HOMO) and HOMO-1, respectively, and occupations of the other Cu AO's in the frontier orbitals are small. The overlap of the Cu $4s$ orbital to the Ag $5s$ orbitals

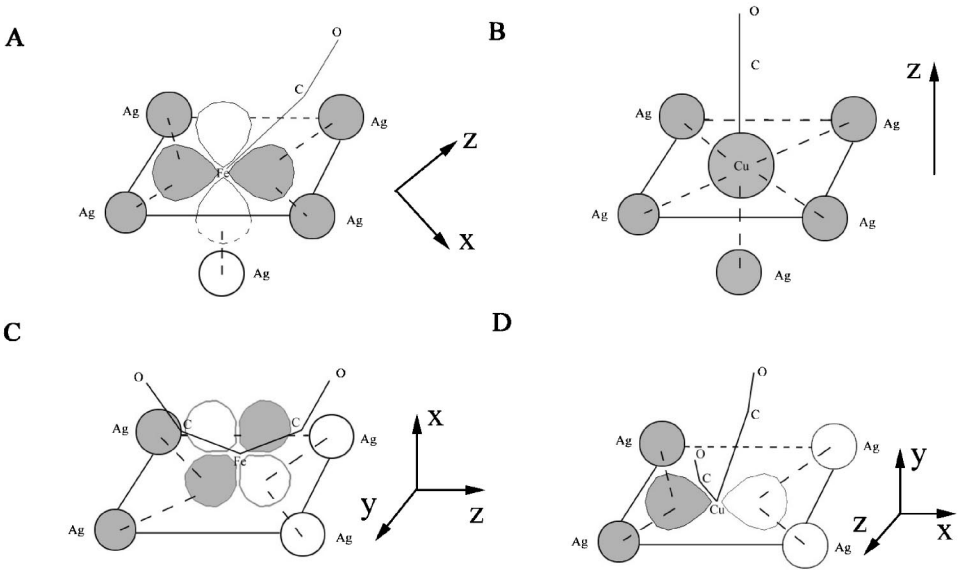

FIG. 2. Metal atomic orbitals in the frontier orbitals of the metal carbonyls which contribute most to the bonding with Ag(110). (A) $Fe(CO)Ag_{21}$ (TL geometry). (B) $Cu(CO)Ag_{21}$ (TS geometry). (C) $Fe(CO)_2Ag_{21}$ (SL geometry). (D) $Cu(CO)_2Ag_{21}$ (SS geometry).

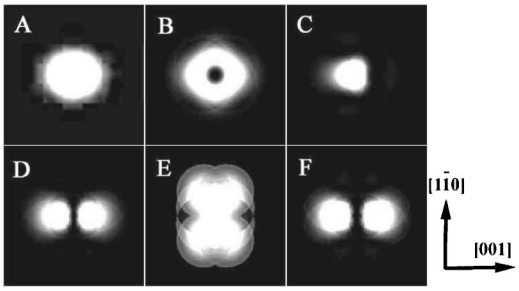

FIG. 3. Simulated STM images of the systems on Ag(110). (A) Fe. (B) CO. (C) Fe(CO). (D) $Fe(CO)_2$. (E) Cu(CO). (F) $Cu(CO)_2$.

is nearly independent of the adsorption orientations. Bonding of the Cu $3d_{z^2}$ orbital to the Ag $5s$ orbitals maximizes at the Per orientation, but the preference is rather small because the waist part of this orbital is slim. This agrees with the calculated data in that the energy differences of Cu(CO)/Ag(110) at different orientations are only several tens of meV. The Fe $3d_{xz}$ orbital in Fe(CO) has a weight of 71% in the HOMO-1 and can distinguish the three orientations markedly due to its diffusive distribution, optimizing the TL orientation. So the energies of Fe(CO)/Ag(110) at different adsorption orientations differ markedly by several hundred meV. Although the Fe $4s$ and $3d_{z^2}$ orbital occupy 36% and 49% in the HOMO, their influence on distinguishing the three orientations is overwhelmed. As to $Fe(CO)_2/Ag(110)$, if we define the x direction as the [110] direction, the overlap between the Fe $3d_{yz}$ orbital and the Ag orbitals is invariant at the SL and SS orientations, while the overlap between the Fe $3d_{xz}$ orbital and the Ag orbitals prefers the SL orientation. Analogously, for $Cu(CO)_2/Ag(110)$, if we define the y direction as the [110] direction, the contribution of the Cu $3p_y$ orbital to distinguishing the orientations vanishes, but the Cu $3p_x$ orbital illuminates the SS orientation. The sketch maps are shown in Fig. 2.

Lee and Ho recorded the STM images of Fe, CO, Fe(CO), $Fe(CO)_2$, Cu(CO), and $Cu(CO)_2$ at 70-mV sample bias and 0.1 nA.[17,18] The images of Fe, CO, and Cu(CO) are round, while those of Fe(CO), $Fe(CO)_2$, and $Cu(CO)_2$ had one or two C_2 axes. We adopted Tersoff and Hamann's formula and its extension[27] to simulate STM images. The electronic structure is calculated using the LDA. For the CO system, we modeled it as a $COAg_{10}$ cluster in which the CO is on the top site of a Ag atom. To avoid the artificial effect from the unsaturated Ag atoms, we chose the likely orbitals in which the atomic orbitals of *M*, C, and O have relatively big contributions, and calculated the partial density of states (PDOS) of the systems. By keeping a constant vertical distance between the tip and the O atom, we plotted the isoheight PDOS as the STM images. The simulated images are presented in Fig. 3. Except for the dark lateral stripes of the simulated image of Cu(CO) which are inevitable within this framework, qualitative agreement of the experimental and simulated images is generally good. We note that although the geometries of $Fe(CO)_2$ and $Cu(CO)_2$ are different (SL and SS), their STM images are alike in that there are bright areas parallel to the [001] direction and dark areas parallel to the [1$\bar{1}$0] direction.

Employing STM-IETS, Lee and Ho measured the C-O stretch frequencies of Fe(CO), $Fe(CO)_2$, Cu(CO), and $Cu(CO)_2$, and the CO-frustrated rotational frequencies of Cu(CO) and $Cu(CO)_2$.[17,18] They also measured some isotopic shifts of the frequencies. These data showed great progress for single-molecule characterization and put forward a challenging question to the computational scientists.

As benchmarks, the frequency of isolated CO is calculated by DMOL with the LDA and GGA. The LDA result is 266.6 meV ($1\ meV = 8.065\ cm^{-1}$) and agreed well with the experimental value 266 meV.[28] The GGA result is 261 meV. Although the GGA can generally give more reliable binding energies than the LDA does, it is not statistically better in predicting the vibrational frequencies. So we only utilize the LDA in the frequency calculations. To compute the frequencies of $M(CO)$ and $M(CO)_2$, we construct the second-derivative matrices of *M*, C, and O with 9 and 15 dimensions, respectively. The matrix elements are $u_{ij} = (\partial^2 E/\partial x_i \partial x_j)(m_i m_j)^{-1/2}$, where E is the binding energy, and x and m are the coordinate and mass of the atom. Second derivatives are calculated by taking finite differences of analytical first derivatives. The gradients are calculated for the geometries with atoms displaced along the 9 or 15 degrees of freedom (the Ag atoms are fixed). The typical values of displacements are ± 0.01 bohr. Diagonalizations of the matrices give all the available frequencies and normal modes. Thus we not only obtain computational frequencies comparable with the experimental values, but also explain the difference between the C-O stretch frequency of $Fe(^{12}C\text{-}^{16}O)_2$ and that of $Fe(^{12}C\text{-}^{16}O)(^{13}C^{18}O)$, and so on. The results are listed in Table III. The biggest absolute error is 8 meV, corresponding to a relative error of about 3%.

We have performed the symmetry assignments for all calculated vibrational states in Table III. According to the irreducible representations of the point groups C_s and C_{2v}, only the A' of C_s and A_1 of C_{2v} modes are dipole active. Therefore, it is easily understood that the C-O stretch modes were recorded in Lee and Ho's experiment since they are dipole active, while the $M(CO)$ frustrated rotational (FR) and frustrated translational (FT) modes were not recorded because they are not dipole active. The reason for no *M*-CO and *M*-Ag stretch modes recorded experimentally is that these modes are dipole active, but they are too soft to be observed in experiment given the low count rates and limited resolution available. Some CO FR modes were recorded in the experiment, and we attribute the mechanism to that these modes might be impact scattering active.[29,30]

In a like manner, we investigated the geometries and the C-O stretch frequencies of the analogous systems with the metal atom as Co, Ni, Zn, and Ag. The results are shown in Table IV. It is found that the six metals can be divided into two classes. Those metal atoms with unfully occupied *d* orbitals (Fe, Co, and Ni) correspond to the TL geometry for $M(CO)$ and the SL geometry for $M(CO)_2$, and the others (Cu, Zn, and Ag) correspond to the perpendicular geometry for $M(CO)$ and the SS geometry for $M(CO)_2$. No TS geometry for $M(CO)$ is found to be the most stable. These results can be also understood using the FOT. Besides, the C-O

TABLE III. Experimental and calculated vibrational frequencies (meV) of molecules adsorbed on Ag(110). The isotopes of Fe and Cu were taken as ^{56}Fe and ^{63}Cu. The *x*, *y*, and *z* directions are the [001], [1$\bar{1}$0], and [110] directions, respectively. The negative values are measured for negative sample bias (Ref. 18).

Mode	Expt.	Calc.	Symmetry	Error
C-O stretch				
Fe(^{12}C-^{16}O)	236	229	A'	−7
Fe(^{13}C-^{18}O)	224	218	A'	−6
Fe(^{12}C-^{16}O)$_2$	234	236	A_1	2
Fe(^{13}C-^{18}O)$_2$	220	225	A_1	5
Fe(^{12}C-^{16}O)(^{13}C^{18}O)	235	235	A'	0
Fe(^{12}C^{16}O)(^{13}C-^{18}O)	223	226	A'	3
Cu(^{12}C-^{16}O)	262	254	A_1	−8
Cu(^{13}C-^{18}O)	249	242	A_1	−7
Cu(^{12}C-^{16}O)$_2$	[e]	249	A_1	[e]
Cu(^{13}C-^{18}O)$_2$	[e]	237	A_1	[e]
Cu(^{12}C-^{16}O)(^{13}C^{18}O)	255	249	A'	−6
Cu(^{12}C^{16}O)(^{13}C-^{18}O)	244	237	A'	−7
^{12}C-^{16}O	261	261	A_1	0
^{13}C-^{18}O	[e]	249	A_1	[e]
M-CO stretch				
Fe-(^{12}C^{16}O)	[e]	70	A'	[e]
Fe-(^{13}C-^{18}O)	[e]	68	A'	[e]
Cu-(^{12}C^{16}O)	[e]	58	A_1	[e]
Cu-(^{13}C^{18}O)	[e]	56	A_1	[e]
CO FR[c]				
Fe(^{12}C^{16}O) (*xz*)	[e]	42	A'	[e]
Fe(^{12}C^{16}O) (*y*)	[e]	32	A''	[e]
Fe(^{13}C^{16}O) (*xz*)	[e]	40	A'	[e]
Fe(^{13}C^{18}O) (*y*)	[e]	31	A''	[e]
Cu(^{12}C^{16}O) (*x*)	36(−32)	39	B_1	[e]
Cu(^{12}C^{16}O) (*y*)	36(−32)	31	B_2	[e]
Cu(^{13}C^{18}O) (*x*)	34(−31)	37	B_1	[e]
Cu(^{13}C^{18}O) (*y*)	34(−31)	30	B_2	[e]
Cu(^{12}C-^{16}O)(^{13}C^{18}O)	35.5(−34.3)[a]	38 37 32[b]	A'' A' A''	[e]
Cu(^{12}C^{16}O)(^{13}C-^{18}O)	34.8(−33.8)[a]	38 37 32[b]	A'' A' A''	[e]
M-Ag(110) stretch				
Ag-Fe(^{12}C^{16}O)	[e]	17	A'	[e]
Ag-Fe(^{13}C^{18}O)	[e]	16	A'	[e]
Ag-Cu(^{12}C^{16}O)	[e]	16	A_1	[e]
Ag-Cu(^{13}C^{18}O)	[e]	16	A_1	[e]
M(CO) FR				
Cu(^{12}C^{16}O) (*x*)	[e]	18	B_1	[e]
Cu(^{12}C^{16}O) (*y*)	[e]	10	B_2	[e]
Cu(^{13}C^{18}O) (*x*)	[e]	18	B_1	[e]
Cu(^{13}C^{18}O) (*y*)	[e]	10	B_2	[e]
M(CO) FT[d]				
Fe(^{12}C^{16}O)	[e]	11	A''	[e]
Fe(^{13}C^{18}O)	[e]	11	A''	[e]

[a]The experimental measurements were recorded beyond the ^{12}C-^{16}O bond and the ^{13}C-^{18}O bond, respectively. However, all the calculatedfrequencies nearby are concerned with simultaneous vibrations of the two bonds.

[b]38 meV: out-of-phase FR(*x*).0.37 meV: out-of-phase FR(*yz*).0.32 meV: in-phase FR(*x*).

[c]FR: frustrated rotation.

[d]FT: frustrated translation.

[e]Not experimentally measured yet.

TABLE IV. Calculated equilibrium geometries, LDA binding energies (eV), and ^{12}C-^{16}O stretch frequencies (meV) of $M(CO)$ and $M(CO)_2$ (M = Fe, Co, Ni, Cu, Zn, Ag) adsorbed on Ag(110).

	$M(CO)$			$M(CO)_2$		
M	Geometry	E_b	Frequency	Geometry	E_b	Frequency
Fe	TL	−62.64	229	SL	−78.32	236
Co	TL	−63.72	234	SL	−79.55	240
Ni	TL	−64.20	248	SL	−79.53	244
Cu	Per	−61.23	254	SS	−75.36	249
Zn	Per	−58.90	250	SS	−72.48	250
Ag	Per	−59.98	256	SS	−73.44	249

stretch frequencies for Fe, Co, and Ni are less than those for Cu, Zn, and Ag. These theoretical predictions may be tested by future experiments.

Lee and Ho's experiments showed the wide possibility of selectively bond formation and characterization.[17,18] By simulating the actual systems as clusters and using the LDA, good predictions for the geometries, vibrational frequencies, and STM images can be acquired. The calculations of relatively accurate vibrational frequencies are the emphasis of this work. We study four other metals and note that all six metals can be divided into two classes owing to whether the *d* orbitals are fully occupied. We manifest the power of the first-principles calculations for the STM-induced single-molecule physics and chemistry.

This work is partially supported by the National Project for the Development of Key Fundamental Sciences in China (G1999075305), by the National Natural Science Foundation of China, by the Foundation of Ministry of Education of China, and by the Foundation of the Chinese Academy of Science. The HPCC, NSC, and SC&CG Laboratory of USTC are acknowledged for computational facilities.

*Corresponding author. Electronic address: jlyang@ustc.edu.cn

[1] F. F. Crim, Science **249**, 1387 (1990).
[2] A. P. Peirce, M. A. Dahleh, and H. Rabitz, Phys. Rev. A **37**, 4950 (1988).
[3] G. Binnig, H. Rohrer, and E. Weibel, Phys. Rev. Lett. **49**, 52 (1982).
[4] D. M. Eigler and E. K. Schweizer, Nature (London) **344**, 524 (1990).
[5] M. F. Crommie, C. P. Lutz, and D. M. Eigler, Science **262**, 218 (1993).
[6] L. Bartels, G. Meyer, and K.-H. Rieder, Phys. Rev. Lett. **79**, 697 (1997).
[7] J. K. Gimzewski and C. Joachim, Science **283**, 1683 (1999).
[8] R. S. Becker, G. S. Higashi, Y. J. Chabal, and A. J. Becker, Phys. Rev. Lett. **65**, 1917 (1990).
[9] D. M. Eigler, C. P. Lutz, and W. E. Rudge, Nature (London) **352**, 600 (1991).
[10] L. Bartels, M. Wolf, T. Klamroth, P. Saalfrank, A. Kühnle, G. Meyer, and K.-H. Rieder, Chem. Phys. Lett. **313**, 544 (1999).
[11] B. C. Stipe, M. A. Rezaei, and W. Ho, Science **279**, 1907 (1998).
[12] B. C. Stipe, M. A. Rezaei, and W. Ho, Phys. Rev. Lett. **81**, 1263 (1998).
[13] B. C. Stipe, M. A. Rezaei, W. Ho, S. Gao, M. Persson, and B. I. Lundqvist, Phys. Rev. Lett. **78**, 4410 (1997).
[14] G. Dujardin, R. E. Walkup, and Ph. Avouris, Science **255**, 1232 (1992).
[15] B. C. Stipe, M. A. Rezaei, and W. Ho, Science **280**, 1732 (1998).
[16] B. C. Stipe, M. A. Rezaei, and W. Ho, Phys. Rev. Lett. **82**, 1724 (1999).
[17] H. J. Lee and W. Ho, Science **286**, 1719 (1999).
[18] H. J. Lee and W. Ho, Phys. Rev. B **61**, R16 347 (2000).
[19] S. H. Vosko, L. Wilk, and M. Nusair, Can. J. Phys. **58**, 1200 (1980).
[20] A. D. Becke, J. Chem. Phys. **88**, 2547 (1988).
[21] J. P. Perdew and Y. Wang, Phys. Rev. B **45**, 13 244 (1992).
[22] DMOL Version 960, Density Functional Theory electronic structure program, Molecular Simulations Inc., 1996.
[23] P. S. Bagus and C. Wöll, Chem. Phys. Lett. **294**, 599 (1998).
[24] M. A. van Daelen, Y. S. Li, J. M. Newsam, and R. A. van Santen, J. Phys. Chem. **100**, 2279 (1996).
[25] The lattice parameter of the Ag fcc structure is 4.09 Å [from C. Kittel, *Introduction to Solid State Physics* (Wiley, New York, 1996), p. 23]. The interlayer spacing between the first and second layers of the Ag(110) surface shrinks by 8% (p. 556). We used these data to initialize the geometries.
[26] R. Hoffmann, *Solids and Surfaces: A Chemist's View of Bonding in Extended Structures* (VCH, Verlag GmbH, 1988).
[27] J. Tersoff and D. R. Hamann, Phys. Rev. B **31**, 805 (1985).
[28] R. T. Lagemann, A. H. Nielsen, and F. P. Dickey, Phys. Rev. **72**, 284 (1947).
[29] N. Lorente and M. Persson, Phys. Rev. Lett. **85**, 2997 (2000).
[30] N. Lorente, M. Persson, L. J. Lauhon, and W. Ho, Phys. Rev. Lett. **86**, 2593 (2001).